Title: Artificial miRNAs reduce human mutant Huntingtin throughout the striatum in a transgenic sheep model of Huntington's disease

Authors: Edith L. Pfister[1]*, Natalie DiNardo[1], Erica Mondo[2], Florie Borel[3], Faith Conroy[1], Cara Fraser[4], Gwladys Gernoux[3], Xin Han[5], Danjing Hu[5], Emily Johnson[1,6], Lori Kennington[1], PengPeng Liu[5], Suzanne J. Reid[7], Ellen Sapp[8], Petr Vodicka[8,9], Tim Kuchel[4], A. Jennifer Morton[10], David Howland[11], Richard Moser[12], Miguel Sena-Esteves[3], Guangping Gao[3], Christian Mueller[3,14], Marian DiFiglia[8], Neil Aronin[1,13]*

Affiliations:

[1]Department of Medicine, University of Massachusetts Medical School, Worcester, MA.

[2]Department of Neurobiology, University of Massachusetts Medical School, Worcester, MA.

[3]Horae Gene Therapy Center, University of Massachusetts Medical School, Worcester, MA.

[4] Preclinical, Imaging and Research Laboratories, South Australian Health and Medical Research Institute, Gilles Plains, South Australia.

[5]West China School of Medicine, West China hospital, Sichuan University. Chengdu, Sichuan Province, China.

[6]Geisel School of Medicine, Dartmouth College, Hanover, NH 03755, USA.

[7]School of Biological Sciences, University of Auckland, Auckland, New Zealand.

[8]MassGeneral Institute for Neurodegenerative Disease, 114 16th Street, Charlestown, MA 02129.

[9]Research Center PIGMOD, Institute of Animal Physiology and Genetics of the Czech Academy of Sciences, Libechov, 27721, Czech Republic

[10]Department of Physiology, Development and Neuroscience, University of Cambridge, Cambridge CB2 3DY, United Kingdom.

[11]CHDI Foundation/CHDI Management, 155 Village Blvd., Princeton, NJ, 08540.

[12]Department of Neurosurgery, University of Massachusetts Medical School, Worcester MA.

[13]RNA Therapeutics Institute, University of Massachusetts Medical School, 368 Plantation Street, Worcester, MA 01605.

[14]Department of Pediatrics, University of Massachusetts Medical School, Worcester MA

*To whom correspondence should be addressed: edith.pfister@umassmed.edu and neil.aronin@umassmed.edu

Work was done at the University of Massachusetts Medical School in Worcester, MA, USA and at the Preclinical, Imaging and Research Laboratories, South Australian Health and Medical Research Institute, Gilles Plains, South Australia.

Short Title: Silencing of human Huntingtin in transgenic sheep

Abstract: Huntington's disease (HD) is a fatal neurodegenerative disease caused by a genetic expansion of the CAG repeat region in the huntingtin (*HTT*) gene. Studies in HD mouse models have shown that artificial miRNAs can reduce mutant HTT but evidence for their effectiveness and safety in larger animals is lacking. HD transgenic sheep express the full-length human *HTT* with 73 CAG repeats. We used AAV9 to unilaterally deliver to HD sheep striatum an artificial miRNA targeting exon 48 of the human *HTT* mRNA under control of two alternative promoters-U6 or CβA. The treatment reduced human mutant (m) *HTT* mRNA and protein 50-80% in the striatum at one and six-months post-injection. Silencing was detectable in both caudate and putamen. Levels of endogenous sheep HTT protein were not affected. There was no significant loss of neurons labeled by DARPP32 or NeuN at six months after treatment, Iba1-positive microglia were detected at control levels. We conclude that safe and effective silencing of human mHTT protein can be achieved and sustained in a large animal brain by direct delivery of an AAV carrying an artificial miRNA.

Introduction

Huntington's disease (HD) is a fatal neurodegenerative disease caused by a genetic expansion of the CAG repeat region in the huntingtin (*HTT*) gene. The *HTT* gene, which was discovered in 1993[1], encodes a ~350 kDa protein comprising a 17 amino acid N-terminal region, followed by the CAG repeat, a polyproline repeat region, and a series of α-helical HEAT (Huntingtin, elongation factor 3, protein phosphatase 2A and TOR1) repeats[2]. Gene-silencing therapeutics, which include methods targeting RNA (antisense oligonucleotides, siRNAs, artificial miRNAs) and DNA (CRISPR/Cas9, Zinc finger nucleases) are promising as they are directed to the most proximal cause of HD, the *HTT* mRNA or gene itself. Studies in HD mouse models support the feasibility of reducing the levels of the HD gene and its protein in brain using antisense oligonucleotides, siRNAs, shRNAs and miRNAs [3–12]. Intrathecal delivery of an antisense oligonucleotide against *HTT* is currently being tested for safety in humans [13] but may have limited effect in the caudate-putamen [7]. Long-lasting expression of shRNAs or artificial microRNAs can be achieved in the brain using a viral delivery approach and direct injection with stereotactic methods. Recombinant adeno-associated virus (rAAV) has been shown to safely deliver its cargo to neurons and other cell types in the striatum of mice [14–16]. Compared to an antisense approach, the advantage of AAV is that it is episomal and can be indefinitely active. Promoter choice determines expression levels of the AAV cargo, which may be an important determinant of the safety and silencing activity of potential RNAi therapies for HD [17,18].

A challenge in advancing human gene therapy for HD is scaling of therapeutics to a capacity that is comparable to treating humans. The sheep brain is significantly larger than that of mice and with a structure more similar to humans than are rodents. Recently we showed that AAV-GFP

could be accurately delivered to the neostriatum of normal Dorset sheep using an image guided approach and convection enhanced delivery [19,20]. HD transgenic sheep express the full-length human *HTT* cDNA with 73 CAG repeats from the human *HTT* promoter [21]. They exhibit a slow disease progression. Only a small number of animals have been analyzed to date, but reduced cannabinoid receptor type 1 (CB1) and DARPP-32 immunoreactivity has been reported in a single 7 month old animal.[21] At six months, there is a decrease in gamma-aminobutyric acid A receptor alpha 1 ($GABA_A$ α1) immunostaining in the caudate nucleus and the putamen and a decrease in leu-enkaphalin (Leu-ENK) in the globus pallidus[22]. There are no detectable changes in immunostaining for glial fibrillary acidic protein (GFAP), a marker for astrogliosis, up to 36 months[22]. Sparse cortical huntingtin aggregates appear by 18 months of age and nuclear inclusions have been reported at 36 months[22]. Young animals show no obvious behavioral phenotypes, but subtle disruptions in circadian rhythms appear by 18 months of age.[23] In this study, we report safe and successful targeting of full-length human HTT mRNA in a large animal model of HD, a necessary first step in the treatment of patients with HD.

Materials and Methods

Animals and animal procedures

Merino sheep were bred at the South Australia Research and Development Institute (Rosedale, SA) and transferred to the South Australia Health and Medical Research Institute (Gilles Plains, SA) approximately 3 weeks prior to surgery. The sheep were provided with food and water as needed and were cared for according to the guidelines of the South Australia Health and Medical Research Institute (approval number 146/13) and the Primary Industries and Regions South Australia (10/13) animal ethics committees. Prior to the administration of anesthetic, the animals were fasted overnight for approximately 8 hours. Animals were given a pre-operative physical including heart rate, respiratory rate, temperature and weight. Baseline samples of serum (5ml) and cerebrospinal fluid (CSF) were collected.

The study was conducted in two parts with two different cohorts of sheep. For the first study, forty-one transgenic animals (21 Wethers, 20 Ewes), aged approximately 8 months were injected unilaterally with 300µl of self-complementary AAV9 (scAAV9) vector at a titer of $1x10^{13}$ gc/ml for a total of $3x10^{12}$ genome copies. Animals weighed between 39kg and 55kg at the time of injection. For the second study, fourteen animals aged 14 months were injected with this vector and fourteen with the control vector. At this time, animals weighed between 52kg and 79kg. Gadolinium was added to the vector formulation to allow post-surgical imaging of the injection spread. The animals were moved to the operating room and prepped for surgery. Buprenorpine and carprofen were administered and animals were anesthetized using ketamine and diazepam. Animals were maintained

under isoflurane during the surgery. They were rested in the sphinx position on a foam cushion on folded extremities or with extremities dangling. A stereotactic frame (Kopf, large animal) was used to hold the animal's head in place. Cerebrospinal fluid was collected via lumbar puncture using a 19-gauge spinal tap cannula. The rAAV was delivered directly to the striatum, targeting the internal capsule. The animal's head was shaved, prepped with betadine, and draped with clear plastic. A curvilinear incision was made using a #15 scalpel to expose the bregma. Once the bregma was identified, a 3 – 4mm burr hole was placed 10mm rostral to the bregma and 11mm lateral of the midline using an electric drill. The convection enhanced delivery (CED) cannula (MRI Interventions, Irvine, CA) was secured in the manipulator and primed with agent to be injected to remove air from the line. The dura was opened with a 1.5mm incision using a #11 scalpel and the CED cannula was advanced 25mm from dural surface to the target depth. The outer cannula (1.65mm) sealed the dural incision to prevent CSF leakage during the infusion. The infusion began 5 minutes after cannula insertion to allow for tissue around the tip to stabilize. The infusion rate was set at 3.33µl/minute until a total volume of 300µl was injected. Ten minutes after infusion was completed the cannula was slowly withdrawn and a bone wax plug was used to repair skull and prevent CSF leakage. The wound was cleansed with saline and closed using a 3.0 vicryl suture. Standard anesthesia wake-up and recovery procedure was followed, according to guidelines at the South Australia Health and Medical Research Institute. Post-surgery MRI was performed to determine the spread of gadolinium. One animal from the first study was excluded following surgery because no gadolinium was visible upon imaging and a second animal from the second study was excluded because the gadolinium

appeared to be primarily in the ventricle. After the surgery, the animals were kept under observation for three days and housed indoors for five days. They were then transferred and housed outdoors in paddocks for the remainder of the study. They were monitored visually for signs of distress and changes in behavior throughout the study. Two animals suffered surgical complications, resulting in partial limb paralysis. This was thought to be due to the positioning of the animals under anesthesia. One was euthanized early and one was moved from the six month to the one-month cohort. Animals were weighed periodically throughout the post-injection period and samples of CSF, blood and serum were taken and saved for further analysis.

For cell counts and differentials, blood was collected via jugular venipuncture into a potassium EDTA blood collection tube (Lavender top; LT) and delivered to the Automated Directorate (SA Pathology, Royal Adelaide Hospital, Adelaide, Australia) for a complete blood examination with differential (CBE differential). For clinical chemistry blood was collected via jugular venipuncture into a serum collection tube (red top; RT). The samples were submitted to SA Pathology for multiple biochemical analysis (MBA).

At one and six-months post-injection animals were harvested, with animals being used for either histology or biochemical analysis. Animals were transported to operating table and placed in ventral recumbency while approximately 6ml of CSF was collected. The animal was repositioned in dorsal recumbency. The carotid arteries were exposed and cannulated at a depth of 4cm from the tip of the cannula. The jugular veins were exposed and 200-500 U Heparin/kg were injected into the jugular vein. Five minutes after administering the Heparin, sheep were euthanized by intravenous injection of Lethabarb

(325mg pentabarbitone sodium/ml) at 1 ml/2kg of body weight. The infusion pump was primed with cold 9% NaCl and connected to the carotid cannulas. For immunohistochemical analysis, the animal was perfused with approximately 8 liters of cold 9% NaCl at a pressure of 500mmHg followed by infusion with 8 liters 4% paraformaldehyde at a pressure of 500mmHg. The brain and liver were extracted. The tissues were post-fixed in 4% paraformaldehyde for 24 hours at 4˚C and transferred to 30% sucrose in 1x phosphate buffered saline for a minimum of 14 days at 4˚C

For RNA, protein, and DNA assays, sheep were perfused with cold 9% NaCl as described above. Collection of the peripheral tissue was performed in the following order: liver, adrenal gland, ovaries (if applicable), muscle, and heart. Cross contamination was prevented by the use of different instruments and washing necropsy surfaces with 10% bleach and 70% ethanol. The organ was removed from the body and harvested using a 3mm biopsy punch or cut to size using a scalpel. A total of ten samples were collected from each organ; two samples were snap frozen in liquid nitrogen and eight samples were stored in RNAlater (Sigma-Aldrich) at 4˚C for 24 hours (300µl of RNAlater for liver, muscle and heart samples, 500µl of RNAlater for adrenal gland and ovary samples).

The brain was removed from the skull using an oscillating saw and bone forceps. After extraction, the brain was weighed and placed ventrally in a custom made plexiglass brain matrix (University of Massachusetts Machine Shop). Nine cuts were made to the brain to fully contain the striatum in four 6mm blocks. The first cut was made posterior to the olfactory bulb attachment (approximately 18mm from the beginning of the matrix) and

the subsequent four cuts were made at 6mm intervals (Figure S1A). The striatum was divided into four 6 mm blocks from posterior to anterior: 2p (posterior), 2m1 (medial 1), 2m2 (medial 2) and 2a (anterior). The striatal dissection was performed in the following order: 2p, 2m1, 2a. The striatum in the right (non-injected) hemisphere was dissected first in all blocks and scalpel blade was changed between hemispheres. The dissection was performed in a petri dish on dry ice and care was taken to remove as much white matter from the striatal tissue as possible. Once dissected out, the striatal pieces (caudate and putamen) were split in half; with the medial piece (closest to midline of block) stored in 1ml of RNAlater at 4˚C and the lateral piece snap frozen in liquid nitrogen. The striatal dissection for the six-month cohort in the CBA study was done in a manner to produce four striatal samples from both the caudate and putamen. The dorsal sections (both medial and lateral) were snap frozen in liquid nitrogen and the ventral sections (both medial and lateral) were stored in 1ml of RNAlater at 4˚C. RNAlater was removed after twenty-four hours and samples were stored at -80˚C.

The 2m2 block was generously covered with OCT and frozen in a 2-methylbutane and dry ice bath. The remainder of the 2a, 2m1, and 2p block was frozen in the same manner. Ten cortex samples were taken from each block in a dorsal to ventral manner; two were snap frozen in liquid nitrogen and eight were stored in 1ml RNAlater at 4˚C.

Sectioning of tissue for histological analysis

Prior to tissue sectioning for histological analysis the striatum was isolated from the fixed and sucrose infiltrated brain, generously covered with OCT, and stored at -20˚C for twenty-four hours. Coronal sections measuring 40µm thick were cut with a sliding microtome (Reichert-

Jung Tetrander sliding microtome) through the entire striatum. The sections were stored in 0.01% sodium azide in 1x phosphate buffered saline at 4˚C.

Vector cloning and rAAV9 Production

For the first study, the test vector contained a U6 promoter driving an artificial miRNA based on the endogenous mir155 backbone (AAV9-U6-miR^{HTT}). The artificial miRNA targets human, but not the sheep huntingtin and has previously been described [17]. A chimeric cytomegalovirus enhancer/chicken B-actin (CBA) promoter driving a chimeric intron was included to improve AAV packaging. The control vector (AAV9) contained only the empty CBA promoter and the intron. For the second study, the test vector contained the CMV enhancer and CBA promoter, the intron and the miRNA-155 based artificial miRNA (AAV9-CBA-miR^{HTT}).

For packaging, the rAAV vector plasmid, a packaging plasmid and an adenovirus helper plasmid were co-transfected into HEK 293 cells. The packaging plasmid expresses the regulatory and AAV9 capsid proteins leading to excision, replication and packaging of the recombinant genome from the rAAV vector plasmid into AAV virions. The recombinant viruses were purified by standard CsCl gradient sedimentation and desalted by dialysis

Analysis of Huntingtin mRNA Levels

The RNA levels in the RNAlater preserved samples were analyzed using a branched DNA assay (bDNA)[24]. Samples were processed according to the manufacturer's guidelines for preparation of tissue homogenates from tissues stored in RNAlater

(Affymetrix eBioscience, Quantigene® Sample Processing Kit). The homogenized samples were analyzed according to the manufacturer's guidelines for the bDNA assay (QuantiGene® 2.0 Reagent System). The samples were analyzed with a probe to detect human huntingtin (Human HD, SA-50339 from Quantigene), ovine huntingtin (Sheep Huntingtin, SF-10586 from Quantigene), and ovine calnexin as a housekeeping gene (Sheep Calnexin, SF-10622 from Quantigene). The assay results were measured with a Tecan Infinite M1000 PRO luminometer (integration time set at 200ms).

Vector Genome Distribution

Genomic DNA was extracted from samples that had been snap frozen in liquid nitrogen using the Gentra Puregene Tissue kit (Qiagen). The genomic DNA concentrations were measured using the NanoDrop ONE^{c} spectrophotometer. Droplet Digital PCR (ddPCR, Biorad) was performed according to the manufacturer's recommendations, using 50ng of DNA as input and TaqMan assays detecting a region of the CB promoter common to all vectors and the HPRT reference gene. Results are expressed as vector genome per diploid genome (vg/dg).

Analysis of Huntingtin Protein Levels—Sample preparation

Small pieces of tissue were removed from frozen blocks and homogenized on ice in 200 µl 10mM HEPES pH7.2, 250mM sucrose, 1mM EDTA + protease inhibitor tablet (mini, complete, EDTA-free Roche #11836170001). Samples were sonicated for 10 seconds and protein concentration was determined using the Bradford method (BioRad #500-0006).

Mesoscale Detection Assay (MSD) for mHTT protein

A 96-well QuicPlex standard plate (MSD) was coated with rabbit monoclonal anti-HTT proline 1220 region antibody (D7F7, Cell Signaling, 1:250) in PBS, overnight at 4°C. The plate was washed 3x 10 min with PBST (PBS + 0.05% Tween20) and blocked with 3% bovine serum albumin (BSA) in PBS for 2 hours at RT. After washing 3x 10 min with PBST, technical duplicates of samples with 20 µg of protein in 25 µl of homogenization buffer or blanks (homogenization buffer) were distributed into the plate and incubated overnight at 4°C on an orbital shaker. The plate was washed 3x 10 min in PBST and incubated in secondary/detection antibody mix as follows: For detection of mHTT, mouse monoclonal anti-polyQ antibody MW1 (DSHB) was mixed with anti-mouse SulfoTag detection antibody (MSD) at 1 µg/ml of each antibody in 1% BSA in PBS. 30 µl of detection antibody mix was applied per well and incubated for 3 hours at RT on an orbital shaker. The plate was washed 3x 10 min in PBST and 150 µl of 2x Read Buffer (MSD) was applied per well right before readout on QuickPlex SQ120 (MSD).

Western Blotting

Equal concentrations of protein (25 µg) were separated by SDS-PAGE on 3-8%Tris-Acetate gels (Life Technologies #EA03785BOX) and transferred to nitrocellulose using TransBlot Turbo (BioRad). Blots were blocked in 5% non-fat dry milk in Tris-buffered saline + 0.1% Tween-20 (TBST) for 1 hour and incubated overnight in primary antibody at 4ºC diluted in blocking solution. Primary antibodies used were: anti-poly-Q (MW1, Coriell, 1:500 or 3B5H10, Sigma, 1:1,000), anti-huntingtin (MAB2166, EMD Millipore, 1:1,000 or Ab1, 1:1,000) [25], anti-DARPP32 (#ab40801, Abcam, 1:10,000), anti-actin (A4700, Sigma, 1:1,000), and anti-spectrin (MAB1622, EMD Milliopore, 1:4,000). Blots

were washed in TBST, incubated in peroxidase labeled secondary antibodies (Jackson Immunoresearch) diluted 1:5000 in blocking solution for 1 hour at room temperature, washed in TBST and incubated in SuperSignal West Pico Chemiluminescent Substrate (Pierce #34080). Images were obtained with a CCD imaging system (Alpha Innotech) and Hyperfilm ECL (GE Healthcare). Densitometry was performed on the digital images using ImageJ software (NIH). Statistical analysis was performed using upaired t-tests and results were expressed as mean value for the injected side.

Immunohistochemistry for DARPP32, NeuN, and Iba1

To quantify the DARPP32 positive cells, every twentieth section was incubated for three minutes in 3% hydrogen peroxide in 1x PBS, twenty minutes in 0.5% Triton-X-100, and then four hours in 1.5% normal goat serum (Vector Labs, S-1000) in 1x PBS. Sections were incubated in anti-DARPP32 (AbCam, ab40801, 1:10,000 dilution) in 1.5% normal goat serum overnight at 4˚C. Sections were then incubated in biotinylated goat, anti-rabbit IgG antibody (Vector Labs, AP-1000, 1:200 dilution) in 1x PBS for 10 minutes. The sections were incubated with 2% Elite A and 2% Elite B reagent from the Vectastain Elite ABC Kit (Vector Labs, PK-6100) in 1x PBS for five minutes. The Metal Enhanced DAB kit (ThermoFisher Scientific, 34065) was used to visualize the DARPP32 positive cells. The sections were incubated in 1x 3, 3'-diaminobenzidine in stable peroxide buffer.

To quantify the NeuN positive cells, every twentieth section was incubated for three minutes in 3% hydrogen peroxide in 1x PBS, twenty minutes in 0.5% Triton-X-100, and then overnight in 1.5% normal goat serum (Vector Labs, S-1000) in 1x PBS at 4˚C

overnight. The sections were incubated in anti-NeuN (Chemicon, MAB377, 1:1,000 dilution) in 1.5% normal goat serum for one hour at 4˚C. The sections were then incubated for 40 minutes in a fluorescent AF594 goat, anti-mouse IgG (ThermoFisher Scientific, A-11005, 1:2,000 dilution) to visualize the NeuN positive cells.

To quantify the Iba1 positive cells, every twentieth section was incubated for one hour in a solution of 5% normal goat serum (Vector Labs, S-1000), 1% bovine serum albumin (Sigma, A-3059), 0.2% Triton-X-100, and 0.03% hydrogen peroxide in 1x PBS. The sections were incubated in anti-Iba1 (Wako Chemicals, 019-19741, 1:1,000 dilution) in 5% normal goat serum (Vector Labs, S-1000) and 1% bovine serum albumin (Sigma, A-3059) at 4˚C overnight. Sections were incubated in biotinylated goat, anti-rabbit IgG antibody (Vector Labs, AP-1000, 1:200 dilution) in 1x PBS for ten minutes. The sections were incubated with 2% Elite A and 2% Elite B reagent from the Vectastain Elite ABC Kit (Vector Labs, PK-6100) in 1x PBS for five minutes. The Metal Enhanced DAB kit (ThermoFisher Scientific, 34605) was used to visualize the reaction by incubating section in 1x 3',3-diaminobenzidine in stable peroxide buffer.

The quantification of DARPP32 and Iba1 positive cells in the left and right hemisphere of the brain was done by taking images (20x for DARPP32 and 40x for Iba1) with a Nikon Eclipse E600 microscope of each section. In order to consistently capture images between different sections, the first image was captured in the medial, dorsal edge of the striatum and the stage was moved 0.5cm toward the ventral edge. Once the ventral edge was reached, the stage was moved 0.5cm laterally and 0.5cm dorsally until ten images

were captured. Random numbers were assigned to each image to eliminate bias when quantifying cells. The cells were counted using ImageJ software (NIH).

The quantification of NeuN positive cells was performed using the Nikon Eclipse E600 with a Chiu Technical Corporation Mercury 100-W lamp at 60x. The stereological method used for capturing DARPP32 and Iba1 images was also used to quantify the NeuN positive cells.

The area of the striatum, caudate, and putamen for each section was measured by manually circling the DARPP32 stained regions using ImageJ software (NIH) on the injected and non-injected sides of every twentieth section through the striatum (29-35 sections per side per animal). The observer was blinded to the conditions. Total volume for each region was determined by multiplying the area by the section thickness (40 microns) by the number of sections between slides (20) and adding together for each animal. Statistical analysis was performed using Microsoft excel, paired and unpaired t-tests, n=3 or 4 animals per group.

Results

Vector genome were widely distributed in the neostriatum

We previously reported silencing of an expanded mouse huntingtin in a knock-in model of HD [14] and of the human *mHTT* transgene mRNA in a transgenic mouse model of HD [17]. We unilaterally injected the striatum in two cohorts of HD sheep (study 1 and study 2). In study 1, the sheep were injected at 8-9 months of age with scAAV9-U6-miR^{HTT} (AAV9miR^{HTT}) or scAAV9-CBA-empty (AAV9), where a non-coding sequence is inserted between the promoter and the poly-A signal. In study 2 the sheep were injected at 14 months of age with scAAV9-CBA-miR^{HTT} or scAAV9-CBA-empty (AAV9). The brains were harvested one and six-months after AAV9 administration. Vector genome copies were determined in a subset of regions (Figure S1) by droplet digital PCR (ddPCR, Figure 1). The genome copies were highest in the caudate and putamen on the injected compared to the non-injected side and were at the highest levels in the scAAV9-U6-miR^{HTT} treated group at 1 and 6 months post-injection. Small amounts of vector genome were present in the cortex and liver, but were undetectable in the adrenals (Figure 1).

A single administration of scAAV9-miR^{HTT} reduced the human mutant huntingtin mRNA in caudate and putamen at one and six-months post-injection

We measured *HTT* mRNA in the anterior and medial striatum using a branched DNA assay that specifically recognizes human and not sheep *HTT* mRNA [24]. At one-month post-injection in the medial 1 block (Figure S1), scAAV9-U6-miR^{HTT} (study 1) reduced human *HTT* mRNA by more than 50% in both the caudate and putamen (Figure 2). No significant silencing was detected in

the anterior striatum (Figure 2), which was farthest from the injection site (Figure S1). At six-months post-injection, mRNA silencing was pronounced in the caudate (Figure 2).

At one-month post-injection, AAV9-CβA-miR^{HTT} (study 2) silenced *HTT* mRNA by greater than 50% in the caudate, 35% in the putamen and 20% in the anterior striatum (Figure 2). Six-months post-injection we observed 40-60% silencing in the caudate, up to 40% silencing in the putamen (Figure 2) Interestingly, we observed no silencing in the lateral anterior striatum (area 1) but a non-significant trend towards lowering in the medial anterior striatum (area 2) indicating that there could be differences in silencing within a single block. This may explain some of the observed variability in the data. There was no significant silencing of the endogenous sheep *HTT* mRNA (Figure S2A).

Western blot assay and Meso Scale Discovery (MSD) immunoassay show that AAV9-miR^{HTT} reduced human mutant huntingtin protein in the caudate and putamen

HTT protein was detected by electrochemiluminescence sandwich assay (MSD, Figure 3) [26] and Western blot (Figure 4) in the same sample preparations. Since antibodies that detect mHTT may have different sensitivities and selectivities, we used multiple antibodies: 3B5H10, MAB2166 and MW1 to detect human mHTT protein (Table 1). In the HD transgenic sheep MAB2166 recognizes only human huntingtin and not sheep HTT [22]. 3B5H10 preferentially detects mHTT (mutant HTT) compared to normal HTT and MW1 preferentially recognizes the expanded polyglutamine region in HTT [27] and was used for Western blotting and for detection of mHTT in the MSD assay.

Results with the MSD assay using MW1 for detection showed that scAAV9-U6-miR^{HTT} treatment (study 1) significantly lowered mHTT protein levels in the caudate, putamen, and anterior striatum at one and six-months post-treatment (Figure 3). Western blotting using 3B5H10 indicated that one-month after treatment, miR^{HTT} significantly reduced mHTT protein in the caudate, putamen and anterior striatum when compared to injection with AAV9 lacking the miRNA (Figure 4). At six-months post-treatment there was a significant reduction of mHTT protein in the putamen. Data are summarized in Table 1.

In study 2, the MSD assay showed that AAV9-CβA- miR^{HTT} reduced mHTT protein by greater than 40% in caudate at one-month post-injection and in caudate, putamen and anterior striatum 6 months after treatment (Figure 3). Western blotting using 3B5H10 indicated significant lowering of mHTT in the putamen at one month and in the putamen area 1 and anterior striatum area 1 at six months (Figure 4). Table 1 compares the mean percent lowering of mHTT detected by Western blot with three anti-mHTT antibodies (3B5H10, 2166, and MW1) and by MSD assay. All three antibodies in Western blot analysis detected significant mHTT lowering in multiple neostriatal regions in study 2 (49% to 81%). Results of mHTT lowering by MSD assay were consistent when two samples from the same striatal region were analyzed in study 2. A comparison of the results by Western blots and by MSD assays with MW1 in study 2 are also noteworthy. There was good agreement between these two different methods of mHTT detection in the magnitude of mHTT lowering.

By Western blot analysis, the cortex overlying the AAV9-miR^{HTT} injected striatum did not show a decline in mHTT protein levels compared to the AAV9 injected cortex (Figure S3A) nor was

there a reduction of mHTT protein in caudate or putamen on the contralateral, non-injected side (Figure S3B).

An important question was whether treatment with AAV9-miR^{HTT} against the human HD gene affected the levels of endogenous sheep HTT. We compared directly the levels of the human transgene mHTT with levels of endogenous sheep HTT by Western blot analysis by taking advantage of differences in migration of the two proteins on SDS PAGE (Figure S2B). Western blot analysis with Ab1 antibody, which recognizes HTT1-17, showed that unlike human mHTT, the endogenous sheep HTT was not lowered by treatment with miR^{HTT} (Figure S2B).

DARPP32 labeled neurons and striatal volume were unaffected by miRNA treatment

DARPP32 immunoreactivity can be used as a marker for the presence of medium spiny neurons. To examine the safety of injection of the AAV vectors, we performed immunohistochemistry for DARPP32 (representative images figures S4, S5) and counted the number of DARPP32 positive cells within every twentieth section in the striatum. There was no significant difference between the number of cells in the AAV9-miR^{HTT} treated and AAV9 control treated groups (Table S1). Although there is a trend toward loss of DARPP32 positive cells between 1 and 6 months in the first study, this difference did not reach statistical significance, nor did we detect differences between wild-type and HD animals in study 2. The number of cells staining for NeuN, a marker of neuronal cells also showed no significant difference between groups. Striatal volumes were determined using cross-sectional area measurements of striatum in DARPP32 labeled sections and were found to be unchanged compared to controls after miRNA treatment (Table S2).

A transient increase in activated microglia occurred after direct injection with AAV9-miR^{HTT} and AAV9 control

We examined immuno-histochemical localization of Iba1 (examples are shown in figures S4, S5), a protein which is localized to microglia and upregulated upon their activation [28]. Labeled cells were identified based on morphology as resting or activated microglia (Table S3). Injection of scAAV9-U6-miR^{HTT} or the corresponding control vector increased the number of activated microglia on the injected side at one-month post-treatment. On the non-injected side, activated cells comprise less than 1% of the total number of Iba1 positive cells, whereas on the injected side they are 49%-58% of the total. Six-months after treatment the injected and non-injected sides were indistinguishable. In the second study, we examined the microglial response only at the study end point (6 months). At this time there is a trend toward higher Iba1 positive activated microglia in the AAV9 (control) injected HD sheep when compared to the AAV9 (control) injected wild-type animals, but this did not reach statistical significance. We cannot exclude the possibility that HD and control sheep have a small difference in microglia response at this age, which the current study is not powered to detect. Additional experiments are required to rule out this hypothesis. The number of Iba1 positive activated microglia is small, between 2% and 12% of the total number of Iba1 positive cells and there was no significant difference between any of the groups. The findings suggest that the transitory increase in activated microglia is independent of AAV cargo and can occur with any vector or with surgery alone.

AAV9-miR^{HTT} treatment did not affect blood counts, electrolytes, or liver and kidney function

Blood samples were taken at four times: baseline (pretreatment), 28 (or 30) days, 90 days, and 180 days post treatment. We measured a complete blood count, electrolytes, liver and kidney function tests (Table S4). No meaningful changes in any of these measurements were found between AAV9-miR^{HTT} injected sheep and controls. In addition, there were no differences in weight or normal movement between groups.

Discussion

This study addressed important concerns for therapy of Huntington's disease. First, a single treatment with the scAAV9-miR^{HTT} effectively lowered mutant human huntingtin in the neostriatum of an animal with a large brain. Second, lowering huntingtin mRNA and protein has been reported in rodent models (3,4,6,11), but only a handful of studies focused on the full length mutant huntingtin (11, 26). The transgenic sheep used here is the only large animal with a full-length human mHTT. A critical advantage of this HD model is that additional downstream exons, compared to N-terminal models of disease, are available for miR targeting. Third, mutant human huntingtin reduction could be achieved and sustained with two different promoters, confirming the robustness of the miR^{HTT} activity.

Lowering mutant human huntingtin protein was the goal of the miRNA mediated silencing. This goal was achieved. Mutant human huntingtin mRNA was reduced, but somewhat less consistently than huntingtin protein lowering which was detected by Western blot with multiple antibodies and by MSD assay. We offer several speculations that might account for the more consistent huntingtin protein reduction compared to mRNA. Huntingtin mRNA may have a compartmental distribution in neurons, exhibiting cytoplasmic and nuclear localization or differential distribution to cell bodies and axons or dendrites. These different pools of mRNA may respond to miRNA silencing differently. Furthermore, the cumulative effect of small differences in injection and sampling site may increase the variability of measurements. Samples for mRNA, protein and DNA vector genome analysis were taken from adjacent sites but the block size was reasonably large. We showed that using our method, there can be differences in observed silencing within a single sample block. In future studies, we would recommend

freezing samples in smaller, single use blocks and measuring protein and RNA from the same sample. Finally, mRNA might be less stable and the methods used to measure it less reproducible than protein. These observations highlight the importance of measuring both mRNA and protein, if possible, by more than a single method. Measurements of protein and mRNA represent bulk amounts in brain regions, rather than in individual cells. Huntingtin mRNA estimations in neurons vary[14] and huntingtin protein variance has not been established. In the current study we present a composite of mRNA silencing. Using these measures we cannot determine the extent of mHtt reduction on a cellular or subcellular level.

Within the brain the vector was mainly concentrated near the injection site between the caudate and putamen, indicating that the local spread by convection enhanced delivery surmounted anatomic restraints that might be imposed by the internal capsule. Much lower steady state levels of AAV9 vector genome were detected in the ipsilateral cortex – it will be interesting in a follow-up study to detect vector genome in neurons collected by laser capture. We speculate that a higher amount of AAV9 volume or titer might have huntingtin lowering properties in cortex. The small amount of AAV9 vector genome in the contralateral neostriatum was not associated with mutant huntingtin protein change. Outside of the brain, we detected only a little AAV9 in the liver.

The transgenic HD sheep offer a value-added to study of mutant huntingtin protein lowering. Further characterization of the model, including a detailed analysis of the number of DARPP32 positive neurons and microglia activation, may reveal additional phenotypes which will further enhance the value of the model. However, concerns about huntingtin protein lowering remain. In addition to the human huntingtin transgene, the model has two sheep huntingtin alleles. Our

approach successfully reduced mutant human huntingtin and did not affect the sheep huntingtin. Most current and broadly applicable Htt targeting therapies affect both huntingtin alleles. Allele specific artificial miRNA would require a complex strategy involving generation of multiple AAV-miRs targeted to single nucleotide polymorphism heterozygosities, and would apply to only a subset of patients. A broad artificial miR would reduce the toxic moiety and could be beneficial for all patients but it is not yet clear if long-term elimination of huntingtin is safe [29,30]. A future study in non-human primates with the same miR^{HTT}, which would silence both alleles would help to clarify this issue. In this study, we focused on young sheep that lack huntingtin inclusions or neuronal loss. For the most part, HD is a disease of adults; study of older sheep would have virtue, especially if the HD transgenic sheep were to develop signs of disease or neuropathology.

Acknowledgments

We wish to acknowledge the staff at the Preclinical, Imaging and Research Laboratories, South Australian Health and Medical Research Institute for their help with the study, Eric Mick for help and consultation on the study analysis and members of the Khvorova lab for suggestions on sample collection, study design and the branched DNA assay. **Funding**: Work was supported by CHDI foundation agreement A-5038. **Author contributions**: Design of study (EP, CM, DH, GGao, JM, MD, MS-E, NA, RM). Writing manuscript (EP, MD, NA). Animal care, blood sampling and analysis (CF, TK). Tissue harvesting and collection (EP, EM, SR, CF). Animal Evaluation (AJM). Histology (DHu, EM, ND, PL, XH). Measurement of RNA, protein, vector genome (EP, ES, FB, GG, LK).

Author Disclosure Statement

CM, EP, NA GG (Gao) have filed patents pertaining to this work

References

1. The Huntington's Disease Collaborative Research Group. A novel gene containing a trinucleotide repeat that is expanded and unstable on Huntington's disease chromosomes. Cell 1993;72:971–83.

2. Andrade MA, Bork P. HEAT repeats in the Huntington's disease protein. Nat Genet 1995;11:115–116.

3. DiFiglia M, Sena-Esteves M, Chase K, et al. Therapeutic silencing of mutant huntingtin with siRNA attenuates striatal and cortical neuropathology and behavioral deficits. Proc Natl Acad Sci U S A 2007;104:17204–17209.

4. Boudreau RL, McBride JL, Martins I, et al. Nonallele-specific silencing of mutant and wild-type huntingtin demonstrates therapeutic efficacy in Huntington's disease mice. Mol Ther 2009;17:1053–1063.

5. McBride JL, Pitzer MR, Boudreau RL, et al. Preclinical safety of RNAi-mediated HTT suppression in the rhesus macaque as a potential therapy for Huntington's disease. Mol Ther 2011;19:2152–2162.

6. Cambon K, Zimmer V, Martineau S, et al. Preclinical Evaluation of a Lentiviral Vector for Huntingtin Silencing. Mol Ther Methods Clin Dev 2017;5:259–276.

7. Kordasiewicz HB, Stanek LM, Wancewicz E V., et al. Sustained Therapeutic Reversal of Huntington's Disease by Transient Repression of Huntingtin Synthesis. Neuron 2012;74:1031–1044.

8. Harper SQ, Staber PD, He X, et al. RNA interference improves motor and neuropathological abnormalities in a Huntington's disease mouse model. Proc Natl Acad Sci U S A 2005;102:5820–5825.

9. Rodriguez-Lebron E, Denovan-Wright EM, Nash K, et al. Intrastriatal rAAV-mediated delivery of anti-huntingtin shRNAs induces partial reversal of disease progression in R6/1 Huntington's disease transgenic mice. Mol Ther 2005;12:618–633.

10. Machida Y, Okada T, Kurosawa M, et al. rAAV-mediated shRNA ameliorated neuropathology in Huntington disease model mouse. Biochem Biophys Res Commun 2006;343:190–197.

11. Drouet V, Perrin V, Hassig R, et al. Sustained effects of nonallele-specific Huntingtin silencing. Ann Neurol 2009;65:276–285.

12. Stanek LM, Sardi SP, Mastis B, et al. Silencing mutant huntingtin by adeno-associated virus-mediated RNA interference ameliorates disease manifestations in the YAC128 mouse model of Huntington's disease. Hum Gene Ther 2014;25:461–474.

13. Safety, Tolerability, Pharmacokinetics, and Pharmacodynamics of IONIS-HTTRx in Patients With Early Manifest Huntington's Disease - Full Text View - ClinicalTrials.gov Available from: https://clinicaltrials.gov/ct2/show/NCT02519036. Accessed June 14, 2017.

14. Keeler AM, Sapp E, Chase K, et al. Cellular Analysis of Silencing the Huntington's Disease Gene Using AAV9 Mediated Delivery of Artificial Micro RNA into the Striatum of Q140/Q140 Mice. J Huntingtons Dis;5 . Epub ahead of print 2016. DOI: 10.3233/JHD-160215.

15. Aschauer DF, Kreuz S, Rumpel S. Analysis of transduction efficiency, tropism and axonal transport of AAV serotypes 1, 2, 5, 6, 8 and 9 in the mouse brain. PLoS One 2013;8:e76310.

16. Cearley CN, Vandenberghe LH, Parente MK, et al. Expanded repertoire of AAV vector serotypes mediate unique patterns of transduction in mouse brain. Mol Ther 2008;16:1710–1718.

17. Pfister EL, Chase KO, Sun H, et al. Safe and Efficient Silencing with a Pol II, but Not a Pol lII, Promoter Expressing an Artificial miRNA Targeting Human Huntingtin. Mol Ther Nucleic Acids 2017;7:324–334.

18. Giering JC, Grimm D, Storm TA, et al. Expression of shRNA from a tissue-specific pol II promoter is an effective and safe RNAi therapeutic. Mol Ther 2008;16:1630–1636.

19. van der Bom IMJ, Moser R, Gao G, et al. Finding the striatum in sheep: Use of a multi-modal guided approach for convection enhanced delivery. J Huntingtons Dis 2013;2:41–45.

20. van der Bom IMJ, Moser RP, Gao G, et al. Frameless multimodal image guidance of localized convection-enhanced delivery of therapeutics in the brain. J Neurointerv Surg . Epub ahead of print 2011. DOI: 10.1136/neurintsurg-2011-010170.

21. Jacobsen JC, Bawden CS, Rudiger SR, et al. An ovine transgenic Huntington's disease model. Hum Mol Genet 2010;19:1873–1882.

22. Reid SJ, Patassini S, Handley RR, et al. Further molecular characterisation of the OVT73 transgenic sheep model of Huntington's disease identifies cortical aggregates. J Huntingtons Dis 2013;2:279–295.

23. Jennifer Morton A, Rudiger SR, Wood NI, et al. Early and progressive circadian abnormalities in Huntington's disease sheep are unmasked by social environment. Hum Mol Genet 2014;23:3375–3383.

24. Coles AH, Osborn MF, Alterman JF, et al. A High-Throughput Method for Direct Detection of Therapeutic Oligonucleotide-Induced Gene Silencing In Vivo. Nucleic Acid

Ther 2016;26:86–92.

25. DiFiglia M, Sapp E, Chase K, et al. Huntingtin is a cytoplasmic protein associated with vesicles in human and rat brain neurons. Neuron 1995;14:1075–1081.

26. Macdonald D, Tessari MA, Boogaard I, et al. Quantification Assays for Total and Polyglutamine- Expanded Huntingtin Proteins. 9 . Epub ahead of print 2014. DOI: 10.1371/journal.pone.0096854.

27. Ko J, Ou S, Patterson PH. New anti-huntingtin monoclonal antibodies: implications for huntingtin conformation and its binding proteins. Brain Res Bull 2001;56:319–329.

28. Ito D, Imai Y, Ohsawa K, et al. Microglia-specific localisation of a novel calcium binding protein, Iba1. Mol Brain Res 1998;57:1–9.

29. Wang G, Liu X, Gaertig MA, et al. Ablation of huntingtin in adult neurons is nondeleterious but its depletion in young mice causes acute pancreatitis. Proc Natl Acad Sci U S A 2016;113:201524575.

30. Dietrich P, Johnson IM, Alli S, et al. Elimination of huntingtin in the adult mouse leads to progressive behavioral deficits, bilateral thalamic calcification, and altered brain iron homeostasis. PLoS Genet 2017;13:e1006846.

Figure and Table Legends

Figure 1. AAV vector genomes in control (AAV9) and treated (AAV9miR^{HTT}) treated animals. In brain samples (A), red represents the injected side and blue, the non-injected. Results from liver and adrenals are reported in B. Vector genomes were measured by digital droplet PCR using genomic HPRT as the reference gene. The values are plotted on a log scale.

Figure 2. scAAV9-anti-HTT-6433 reduces human mutant huntingtin mRNA in the striatum. Data shown are the signal for HTT mRNA normalized to sheep calnexin (CANX). Asterisks indicate significant differences in means between treatment groups (AAV9 or AAV9miR^{HTT}) at $p \leq 0.03$ with unpaired t-tests. The U6-promoter driven artificial miRNA significantly lowers human mutant HTT mRNA caudate and putamen at 1 month post-injection and in putamen at 6 months post-injection. The CBA-promoter driven artificial miRNA lowers the HTT mRNA in the caudate, putamen and anterior striatum at 1 month post-injection and in the caudate and putamen at 6 month post-injection. The medial region of the caudate, lateral putamen and anterior striatum were examined in the analysis.

Figure 3. Human mutant HTT levels detected by MSD assay at 1 and 6 months post-injection in study 1 (U6 promoter) and study 2 (CBA promoter). Graph shows distribution of individual values and means (horizontal bars) for sheep treated with either AAV9 (control) or AAV9-miR^{HTT}. Results are shown for different striatal regions (caudate, putamen and anterior striatum). Asterisks * indicate significant difference on the injected side between AAV9 and AAV9-miR^{HTT} at $p<0.05$ based on unpaired t-tests.

Figure 4. Western blot assays show that AAV9-miR^{HTT} reduces the human mutant huntingtin protein in the striatum. A. Sample Western blots of putamen from Studies 1 and 2 show mutant HTT detected with antibody 3B5H10 and actin as loading control. B. Graph shows distribution of individual values and mean (horizontal bar) for sheep treated with either AAV9 (control) or AAV9-miR^{HTT}. Shown are results for different striatal regions (caudate, putamen and anterior striatum) in studies 1 and 2 and 1 and 6 months post-injection. In study 2, 6 months post-injection two areas (Area 1 and 2) were examined in each region. Asterisks indicate significant difference on the injected side between AAV9 and AAV9-miR^{HTT} at $p<0.05$ based on unpaired t-tests.

Table 1. Mean percent of mutant huntingtin protein lowering by Western blot and MSD assays in Studies 1 and 2. The human mutant huntingtin protein was measured by Western blot with anti-htt polyQ antibody 3B5H10 in study 1 and antibodies 3B5H10, MAB2166 (anti-HTT443-456), which does not recognize sheep HTT (Reid et al., 2013), and anti-polyQ monoclonal antibody MW1 in study 2. In the MSD assays MW1 was used as the detection antibody. This table reports the mean percent mHTT lowering for the caudate, putamen, and anterior striatum. Percent lowering was calculated by dividing the average signal for the injected side in the AAV9miR^{HTT} treated sheep by the

average signal for the injected side in the AAV9 alone treated animals. Study 2, 6 months post-injection, 2 areas per region were analyzed. *$p<0.05$, **$p<0.001$, unpaired t test, N= Study 1, 1 month, 6 AAV9, 8 AAV9-miR^{HTT}; Study 1, 6 months, 6 AAV9, 7 AAV9-miR^{HTT}; Study 2, 1 month, 4 AAV9, 4 AAV9-miR^{HTT}; Study 2, 6 months, 6 AAV9, 6 AAV9-miR^{HTT}.

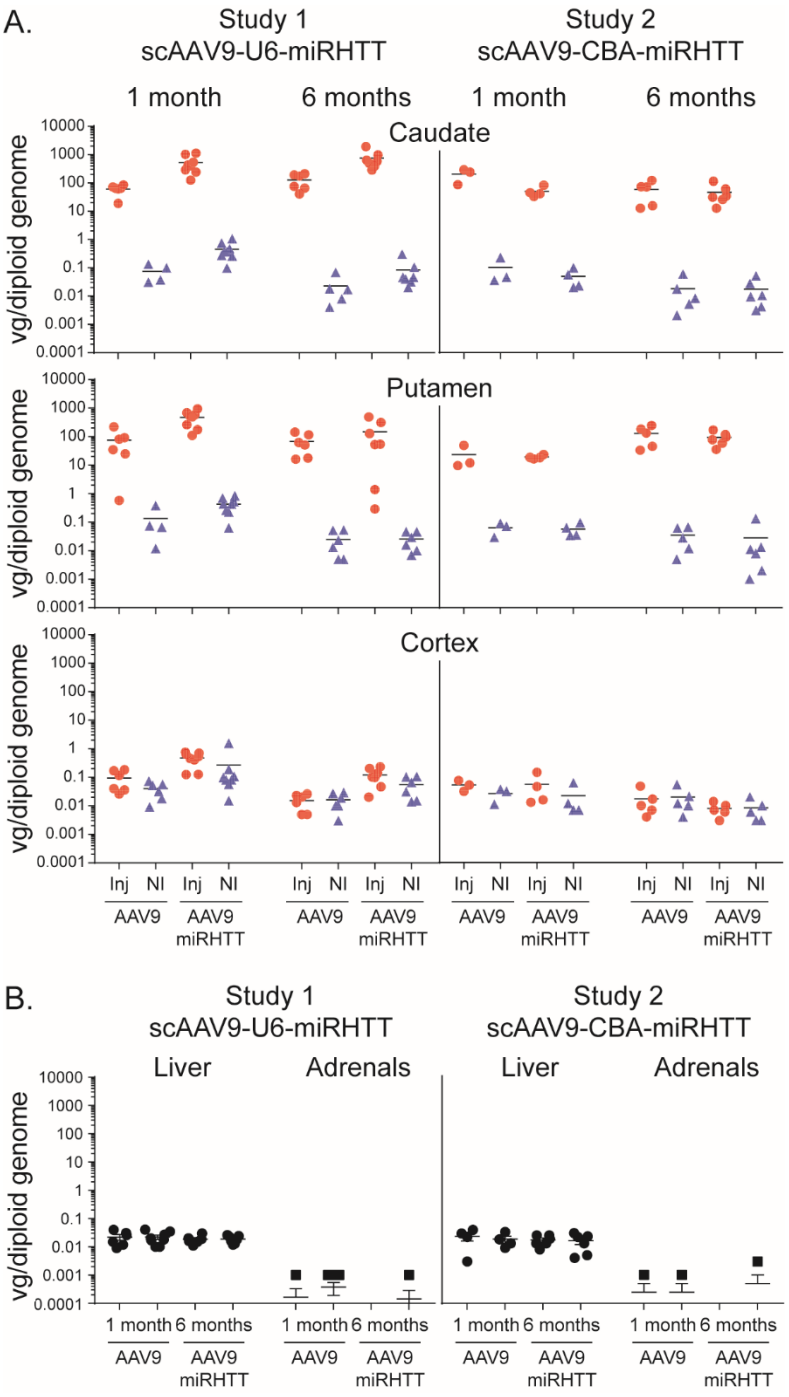
A.
Study 1
scAAV9-U6-miRHTT
Study 2
scAAV9-CBA-miRHTT
1 month
6 months
1 month
6 months
Caudate
Putamen
Cortex
vg/diploid genome
10000
1000
100
10
1
0.1
0.01
0.001
0.0001
Inj
NI
Inj
NI
AAV9
AAV9 miRHTT
B.
Study 1
scAAV9-U6-miRHTT
Study 2
scAAV9-CBA-miRHTT
Liver
Adrenals
Liver
Adrenals
vg/diploid genome
1 month
6 months
AAV9
AAV9 miRHTT

Figure 1.

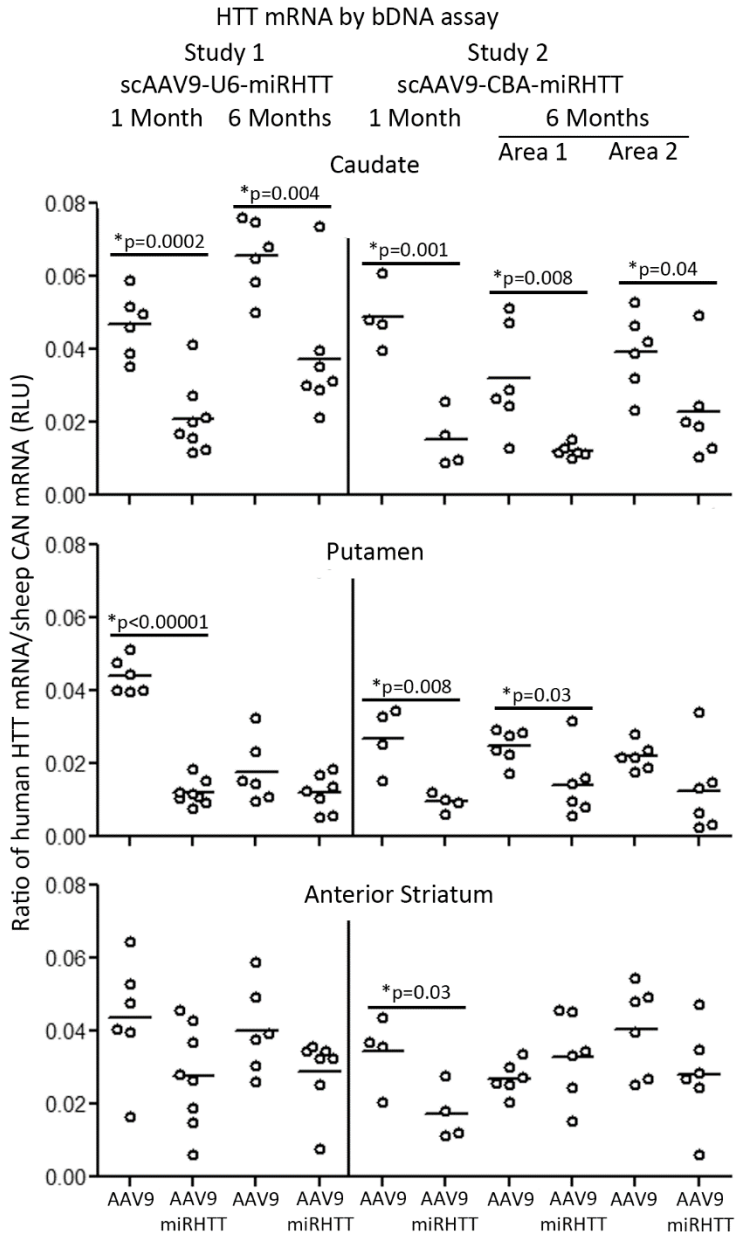
HTT mRNA by bDNA assay
Study 1
scAAV9-U6-miRHTT
1 Month
6 Months
Study 2
scAAV9-CBA-miRHTT
1 Month
6 Months
Area 1
Area 2
Caudate
*p=0.0002
*p=0.004
*p=0.001
*p=0.008
*p=0.04
Putamen
*p<0.00001
*p=0.008
*p=0.03
Anterior Striatum
*p=0.03
Ratio of human HTT mRNA/sheep CAN mRNA (RLU)
0.00
0.02
0.04
0.06
0.08
AAV9
AAV9 miRHTT

Figure 2

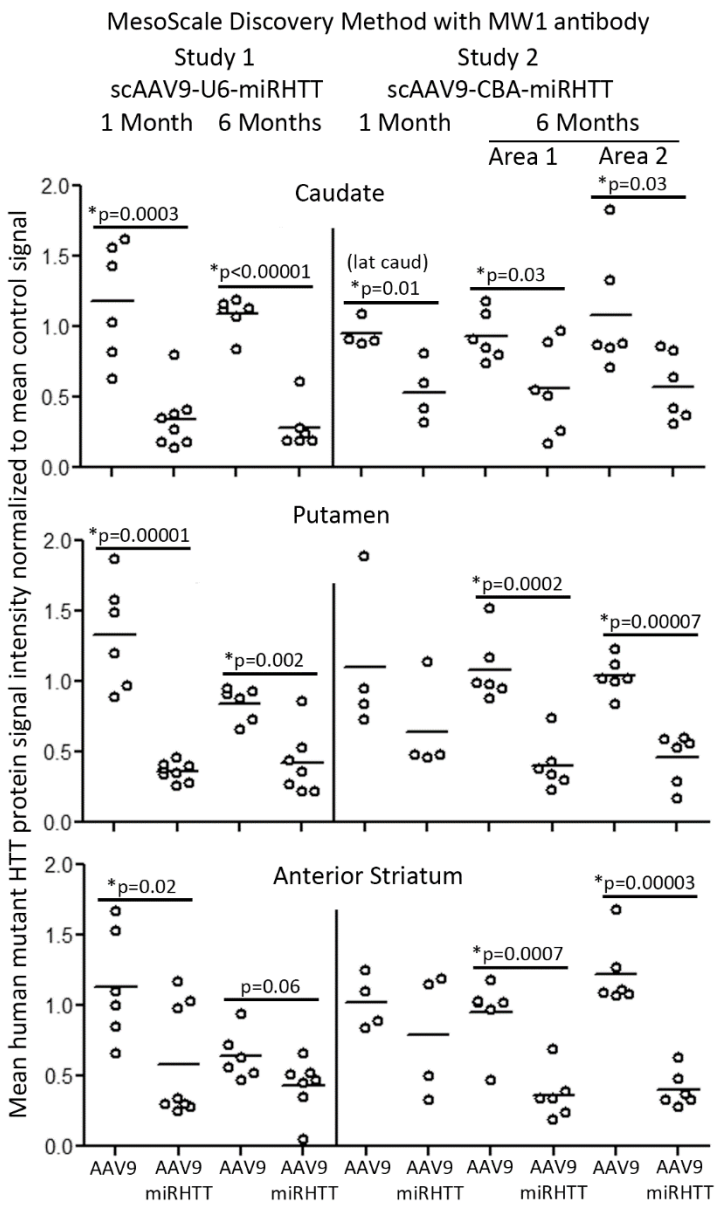
MesoScale Discovery Method with MW1 antibody
Study 1
scAAV9-U6-miRHTT
1 Month
6 Months
Study 2
scAAV9-CBA-miRHTT
1 Month
6 Months
Area 1
Area 2
Caudate
*p=0.0003
*p<0.00001
(lat caud)
*p=0.01
*p=0.03
*p=0.03
Putamen
*p=0.00001
*p=0.002
*p=0.0002
*p=0.00007
Anterior Striatum
*p=0.02
p=0.06
*p=0.0007
*p=0.00003
Mean human mutant HTT protein signal intensity normalized to mean control signal
0.0
0.5
1.0
1.5
2.0
AAV9
AAV9 miRHTT

Figure 3

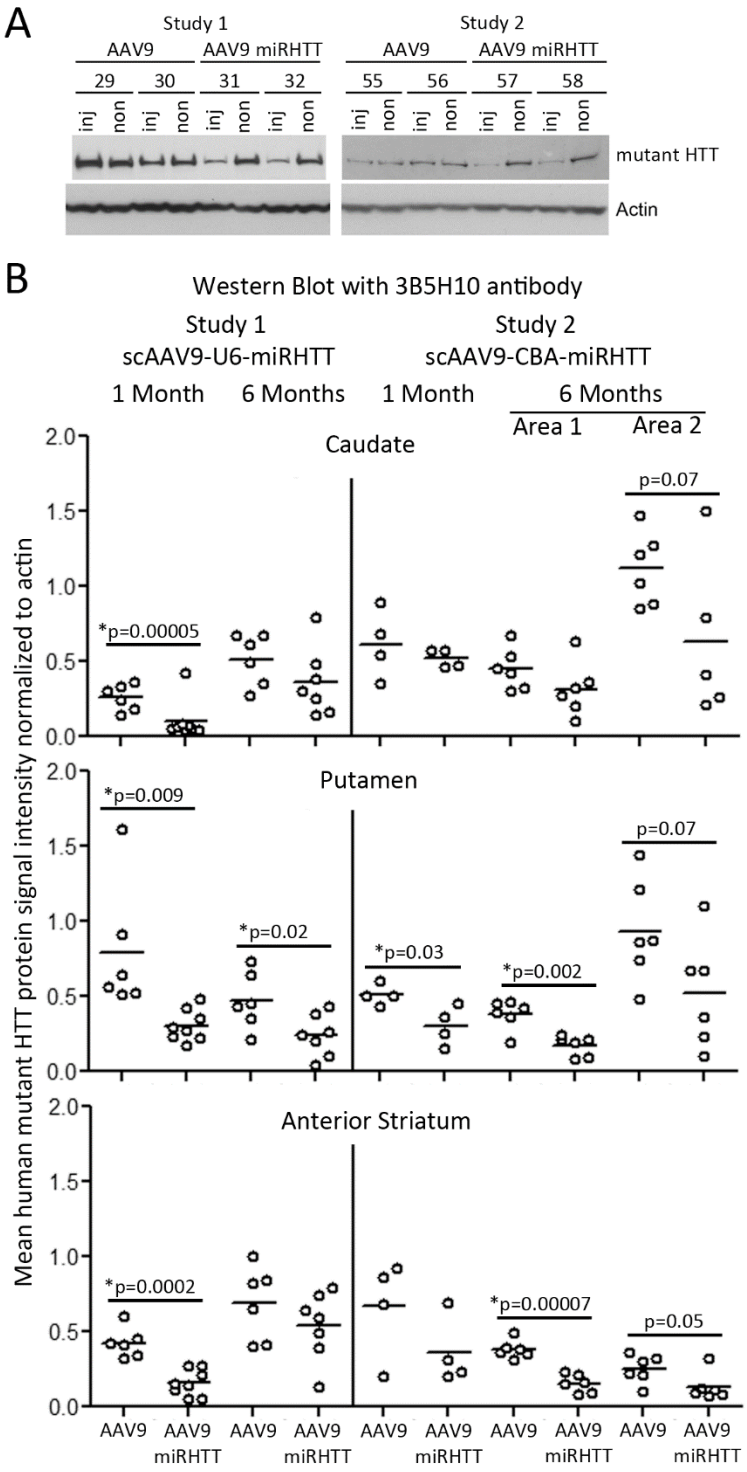
A
Study 1
Study 2
AAV9
AAV9 miRHTT
29
30
31
32
55
56
57
58
inj
non
mutant HTT
Actin
B
Western Blot with 3B5H10 antibody
Study 1
scAAV9-U6-miRHTT
Study 2
scAAV9-CBA-miRHTT
1 Month
6 Months
Area 1
Area 2
Caudate
Putamen
Anterior Striatum
Mean human mutant HTT protein signal intensity normalized to actin
*p=0.00005
p=0.07
*p=0.009
*p=0.02
*p=0.03
*p=0.002
*p=0.0002
*p=0.00007
p=0.05
AAV9
AAV9 miRHTT

Figure 4

Table 1. Mean percent of mutant huntingtin protein lowering by Western blot and MSD assays in Studies 1 and 2. The human mutant huntingtin protein was measured by Western blot with anti-htt polyQ antibody 3B5H10 in study 1 and antibodies 3B5H10, MAB2166 (anti-HTT443-456), which does not recognize sheep HTT (Reid et al., 2013), and anti-polyQ monoclonal antibody MW1 in study 2. In the MSD assays MW1 was used as the detection antibody. This table reports the mean percent mHTT lowering for the caudate, putamen, and anterior striatum. Percent lowering was calculated by dividing the average signal for the injected side in the AAV9miR^{HTT} treated sheep by the average signal for the injected side in the AAV9 alone treated animals.

Table 1. Mean percent of mutant huntingtin protein lowering by Western blot and MSD assays in Studies 1 and 2.												
Study# (promoter)	Study 1 (U6)				Study 2 (CBA)							
Assay mutant htt antibody	Western blot (3B5H10)		MSD MW1		Western blot (3B5H10)		Western blot (MAB2166)		Western blot (MW1)		MSD MW1	
Post-injection Interval (months)	1	6	1	6	1	6	1	6	1	6	1	6
Caudate	78**	30	71**	74**	16	30, 43	61	46, 58*	50*	65*, 70	43*	40*, 47*
Putamen	61*	47*	73**	50*	40*	55*, 44	68*	65*, 67*	54	51*, 56*	42	63**, 56**
Anterior Striatum	63**	22	49*	33	46	60**, 48	46	81*, 62*	-8	74*, 53*	22	62**, 67**

Study 2, 6 months post-injection, 2 areas per region were analyzed.
*p<0.05, **p<0.001, unpaired t test, N= Study 1, 1 month, 6 AAV9, 8 AAV9-miR^{HTT}; Study 1, 6 months, 6 AAV9, 7 AAV9-miR^{HTT}; Study 2, 1 month, 4 AAV9, 4 AAV9-miR^{HTT}; Study 2, 6 months, 6 AAV9, 6 AAV9-miR^{HTT}.

Supplementary Materials

Fig. S1. Schematic of sheep brain dissected in the coronal plane.

Fig. S2. Quantification of artificial miRNA guide strand.

Fig. S3. Levels of endogenous sheep htt mRNA and protein in AAV9 and AAV9miR^{HTT} treated sheep.

Fig S4. Human mutant HTT protein in the cortex, contralateral caudate and putamen.

Table S1. Number of DARPP32 and NeuN positive cells.

Table S2. Striatal volume.

Table S3. Number and classification based on morphology of Iba1 positive cells.

Data file S1. Clinical pathology and complete blood counts for all sheep.

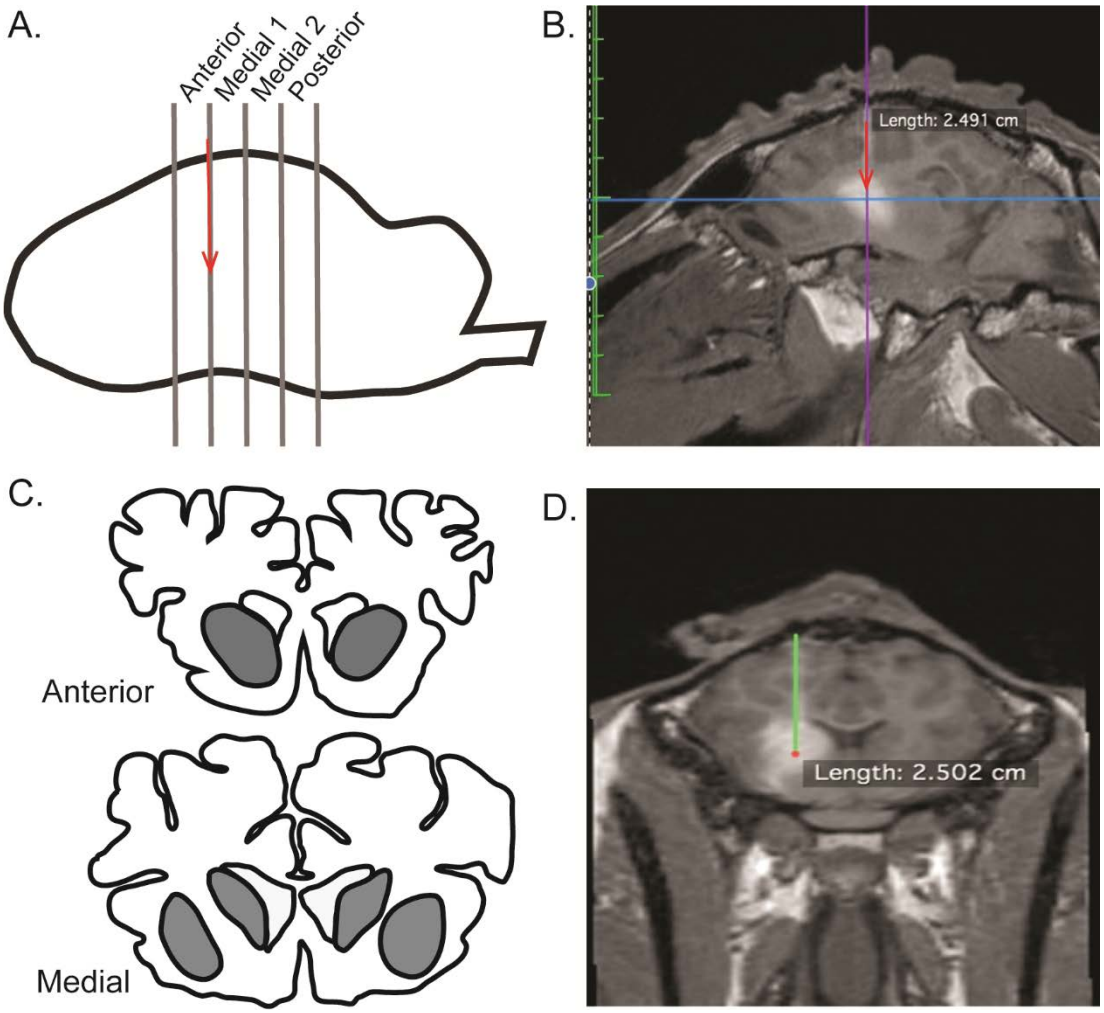

Figure S1. Schematic of sheep brain dissected in the coronal plane. A. The brain was placed in a custom built brain matrix and cuts were made so that the entire striatum was contained within 4, 6mm blocks. The typical trajectory is illustrated in B. Distance is 2.49cm from the dural surface. C. The anterior block contains the anterior portion of the striatum which is not divided by the internal capsule and the medial blocks, to which the injection is targeted have a defined putamen and caudate. D. The green line is the exact trajectory corresponding to the saggital view in B.

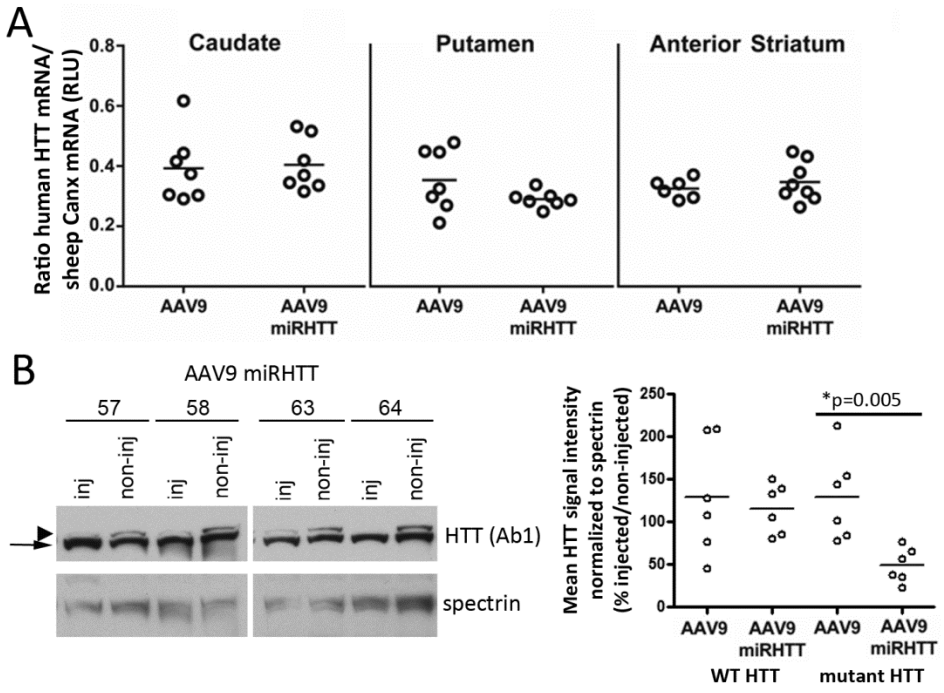

Figure S2. Levels of endogenous sheep htt mRNA and protein in AAV9 and AAV9miR^{HTT} treated sheep. A. Sheep htt mRNA levels were determined as described in methods and are expressed relative to sheep calnexin (Canx). Shown are results from Study 2. There is no difference in endogenous sheep htt mRNA levels between AAV9 and AAV9miR^{HTT} treated groups. B. Levels of endogenous sheep huntingtin and human mHTTprotein detected with anti-htt1-17 antibody (Ab1) in putamen from Study 2, 6 months post-injection. Sample Western blot shows signal for wt htt (arrow) and human mutant htt (arrowhead) for the injected and non-injected sides of the brain in 4 different sheep injected on one side with AAV9miR^{HTT}. Graph shows mean wt sheep htt and human mHTT signals determined from the densitometry as percent injected side to non-injected side. Note that treatment with AAV9miR^{HTT} does not affect levels of endogenous sheep huntingtin protein but significantly reduces levels of human mHTT. Asterisk indicates p=0.005 with unpaired t-test.

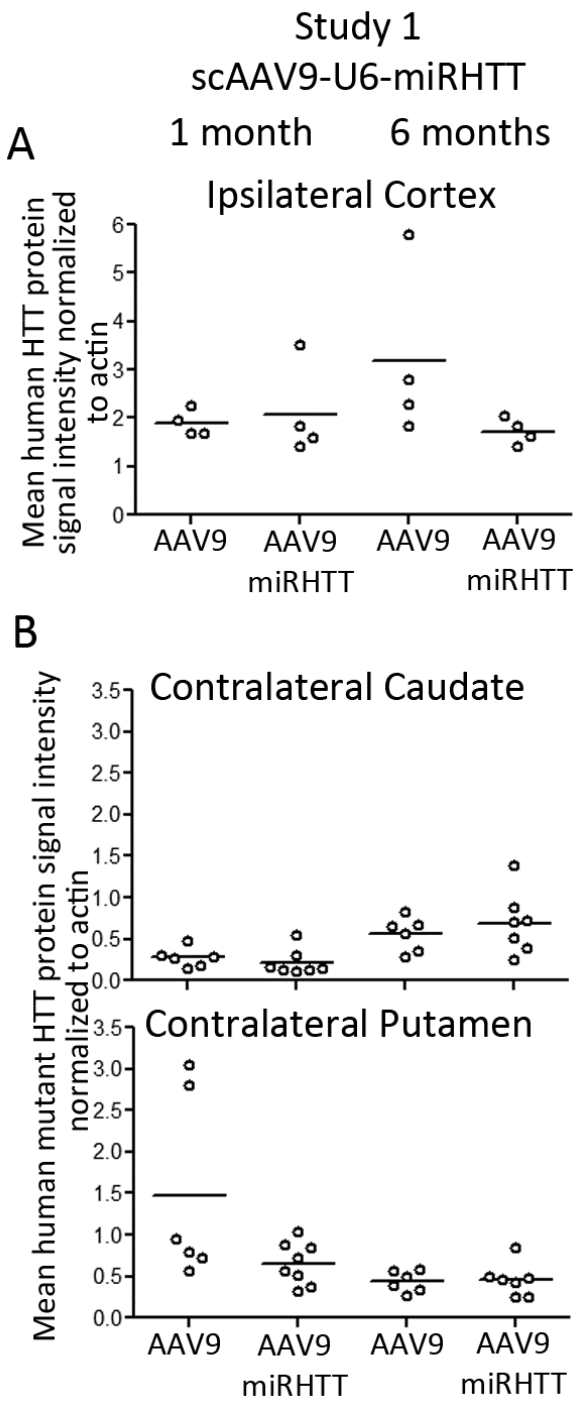

Figure S3. mHTT levels are unchanged in the ipsilateral cortex and contralateral caudate putamen of miR^{HTT} injected sheep striatum A. Graph shows mean levels of mHTT normalized to actin in the cortex ipsilateral to the miR^{HTT} injected striatum. Data are from study 1, 1 and 6 months post-injection, NS, based on unpaired t-test. B, Bar graph shows levels of mHTT normalized to actin in the caudate and putamen contralateral to the miR^{HTT} injected striatum. Data are from study 1, 1 and 6 months post-injection, NS, based on unpaired t-test.

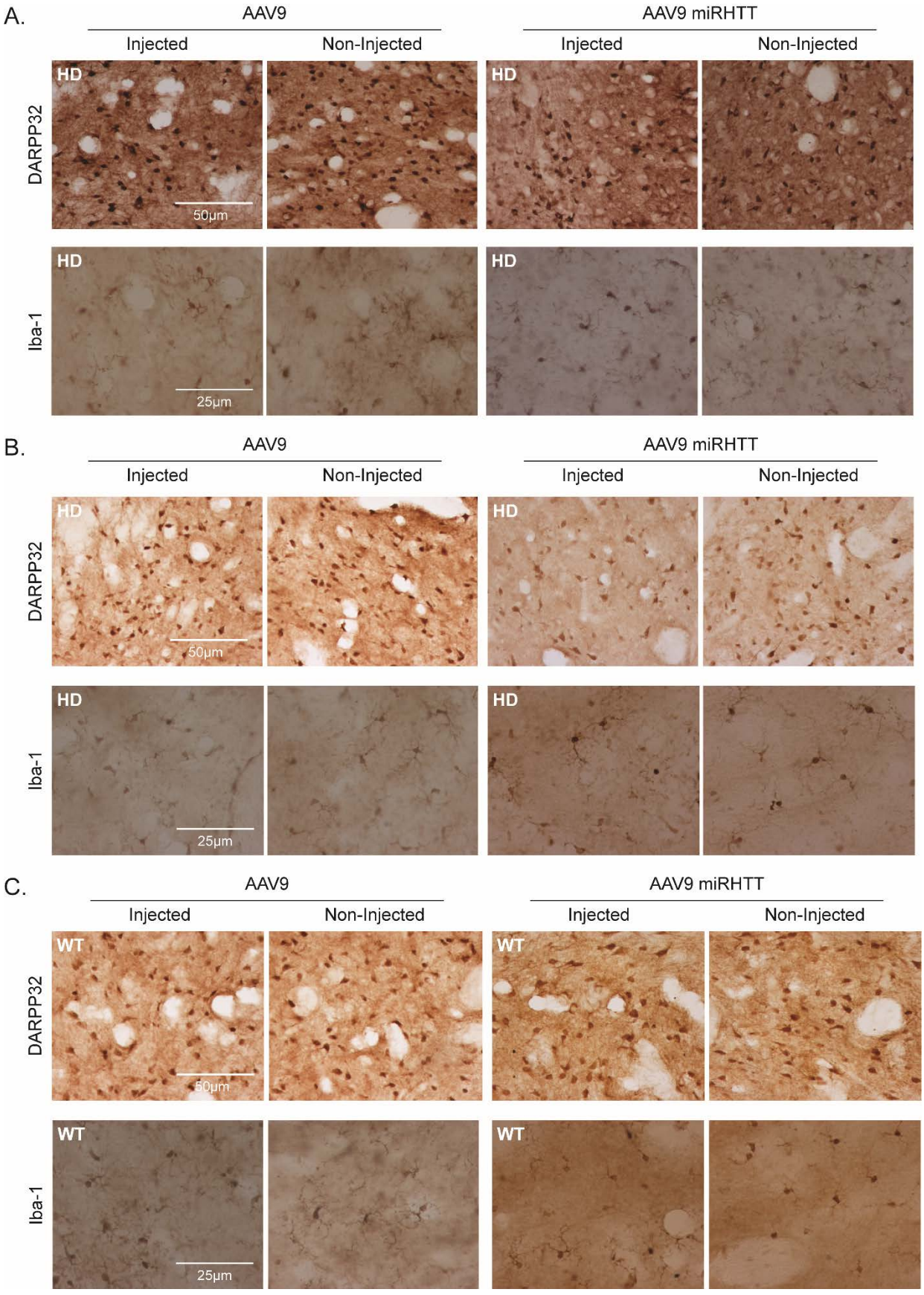
A.
AAV9
AAV9 miRHTT
Injected
Non-Injected
Injected
Non-Injected
DARPP32
HD
HD
50μm
Iba-1
HD
HD
25μm
B.
AAV9
AAV9 miRHTT
Injected
Non-Injected
Injected
Non-Injected
DARPP32
HD
HD
50μm
Iba-1
HD
HD
25μm
C.
AAV9
AAV9 miRHTT
Injected
Non-Injected
Injected
Non-Injected
DARPP32
WT
WT
50μm
Iba-1
WT
WT
25μm

Figure S4. Representative examples of immunohistochemical staining of injected sheep used to count cells in tables S1 and S3. Peroxidase immunohistochemistry with DARPP32 antibody to label medium spiny neurons and the Iba-1 antibody to label microglial cells in the striatum of transgenic and normal sheep. **A.** Study 1 (U6 promoter) transgenic sheep 6 months post injection. **B.** Study 2 (CBA promoter) transgenic sheep 6 months post injection. **C.** Study 2 (CBA promoter) wild type sheep 6 months post injection. We found no differences between groups.

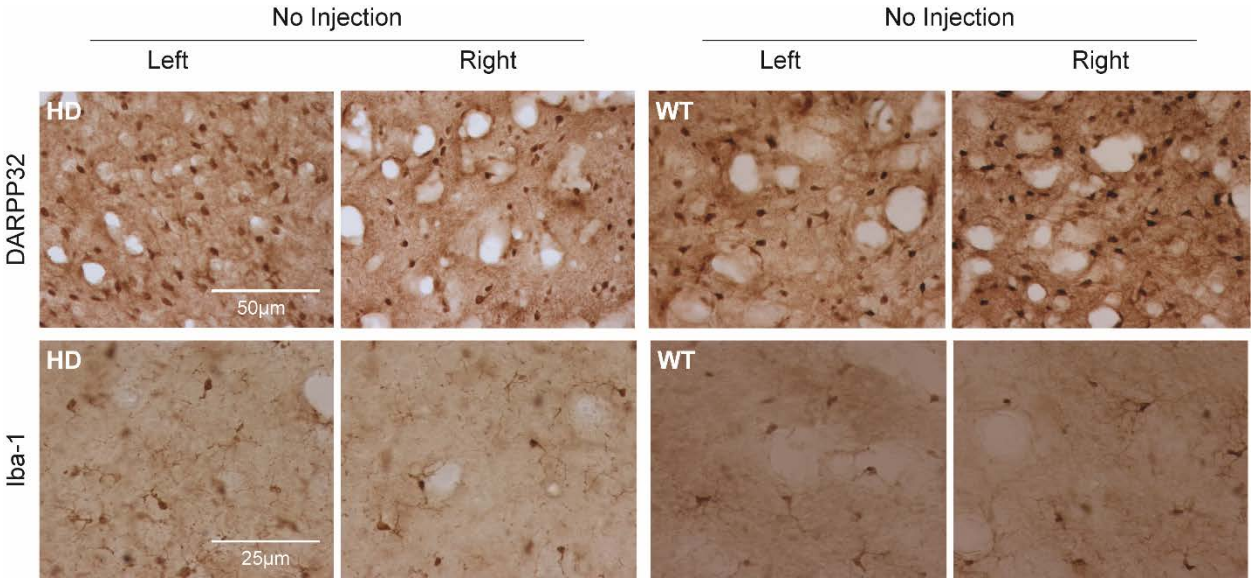

Figure S5. Representative examples of immunohistochemical staining of non-injected sheep used to count cells in tables S1 and S3 Peroxidase immunohistochemistry with the DARPP32 antibody to label medium spiny neurons and the Iba-1 antibody to label microglial cells in the striatum of transgenic and wild type sheep that did not receive an injection. These animals were age-matched to those in the AAV9 and AAV9 miRHTT groups from study 2 (CBA promoter).

Study[#] (promoter)	Group		Post-injection interval (months), number	Side	# of DARPP32 positive cells	# of NeuN positive cells
Study 1 (U6)	HD	AAV9	1 (n=3)	inj	4201±389	
				non-inj	4056±488	
			6 (n=3)	inj	2819±614	1185±70
				non-inj	3314±364	1368±180
		AAV9 miRHTT	1 (n=4)	inj	4327±1444	
				non-inj	4587±838	
			6 (n=3)	inj	3884±1222	1547±315
				non-inj	4149±924	1633±262
Study 2 (CBA)	HD	AAV9	6 (n=3)	inj	2459±85	1111±314
				non-inj	2324±347	1184±330
		AAV9 miRHTT	6 (n=3)	inj	2061±321	1404±61
				non-inj	2084±460	1499±46
		No Injection	6 (n=3)	left	1852±232	1440±76
				right	2047±306	1183±220
Study 2 (CBA)	WT	AAV9	6 (n=3)	inj	2121±96	1157±180
				non-inj	2148±146	1106±86
		AAV9 miRHTT	6 (n=3)	inj	1799±223	1285±151[1]
				non-inj	1895±327	1434±142
		No Injection	6 (n=3)	left	1963±181	1188±328
				right	2101±219	1056±258

Table S1. Number of DARPP32 and NeuN positive cells. Data were analyzed by paired t-test (injected to non-injected side). A significant difference was found between injected and non-injected sides only in WT sheep injected with AAV9-CβA-miR^{HTT} at six-months post injection, [1]p=0.002 by paired t-test.

				Volume (mm3), Mean±SD		
				Study 1 (U6)		Study 2 (CBA)
				1 month post-injection	6 months post-injection	6 months post-injection
Caudate	HD	AAV9	inj	293±54	241±13	
			non-inj	300±48	248±17	
			% inj/non-inj	97.3±4.2	97.2±3.2	
		AAV9 miR^{HTT}	inj	257±48	302±15	280±79
			non-inj	290±48	325±33	304±49
			% inj/non-inj	88.6±9.3	93.8±15	91.1±12
	WT	AAV9 miR^{HTT}	inj			283±67[1]
			non-inj			309±65
			% inj/non-inj			91.4±2.7
Putamen	HD	AAV9	inj	298±46	247±33	
			non-inj	307±52	274±11	
			% inj/non-inj	97.0±1.4	90.3±13	
		AAV9 miR^{HTT}	inj	278±57	318±39[2]	281±10
			non-inj	285±50	340±45	314±21
			% inj/non-inj	97.5±8.9	93.6±1.2	89.9±6.9
	WT	AAV9 miR^{HTT}	inj			292±45
			non-inj			329±63
			% inj/non-inj			89.2±3.7
Striatum (Rostral pole + Caudate + Putamen)	HD	AAV9	inj	1041±172	947±28	
			non-inj	1034±150	1006±49	
			% inj/non-inj	101±2.3	94.3±5.6	
		AAV9 miR^{HTT}	inj	1023±85	1030±31[3]	1165±145
			non-inj	1037±96	1110±31	1222±116

			% inj/non-inj	98.8±4.7	92.8±1.7	95.1±4.0
	WT	AAV9 miR^{HTT}	inj			1159±76
			non-inj			1210±32
			% inj/non-inj			95.7±3.8

Table S2. Striatal volume. Volume was determined from cross-sectional areas of 29-35 40 µm sections per side per animal, N=3 sheep per group. [1]p=0.01, [2]p=0.03, [3]p=0.02, using a paired t test.

Study[#] (promoter)	Group		Post-injection interval (months)	Side	# of Iba1 activated microglia	# of Iba1 resting microglia	Total # Iba1 positive cells
Study 1 (U6)	HD	AAV9	1	inj	253±178	180±102[3]	433±168
				non-inj	2.0±2	305±70	307±68
			6	inj	29±19	351±104	380±123
				non-inj	12±6	377±214	388±219
		AAV9 miR^{HTT}	1	inj	195±2	201±77[4]	396±135
				non-inj	2.8±3	347±116	350±113
			6	inj	29±8[1]	279±202	308±194
				non-inj	6.7±4	311±148	318±144
Study 2 (CBA)	HD	AAV9	6	inj	38±10	263±31	301±23[4]
				non-inj	23±3	248±29	271±32
		AAV9 miR^{HTT}	6	inj	10±4	240±38	251±37
				non-inj	6.0±4	260±32	266±36
		No Injection	6	left	8.3±5	256±90	265±85
				right	13±17	192±112	204±100
Study 2 (CBA)	WT	AAV9	6	inj	16±4[2]	288±39	303±35
				non-inj	7.0±4	256±50	263±46
		AAV9 miR^{HTT}	6	inj	22±18	261±29	283±26
				non-inj	8.7±7	303±59	312±55
		No Injection	6	left	10±12	246±108	256±96
				right	9.3±8	298±63	307±69

Table S3. Number and classification based on morphology of Iba1 positive cells. Statistical analysis was done by paired t-test (injected side vs. non-injected side). A significant increase in activated microglia on the injected side compared to non-injected side was found in HD sheep injected with AAV9-U6-miR^{HTT} ([1] p=0.01) and in WT sheep injected with AAV9 ([2] p=0.006) at six-months. A significant decrease in resting microglia was found at one-month in HD sheep injected with both AAV9 ([3] p=0.05) and AAV9-U6-miR^{HTT} ([4] p=0.04) and a significant increase in total microglia was found in HD sheep injected with AAV9 at six-months in study 2 ([4] p=0.04). All analyses were done by paired t-test comparing injected to non-injected side.

Table S4. Clinical pathology and complete blood counts for all sheep (excel file data S1).